SRTTU

JCARME
ISSN: 2228-7922

Journal of Computational and Applied Research
in Mechanical Engineering
Vol. 7, No. 1, pp. 57-71
jcarme.srttu.edu

Evaluation of combined hardening model in ratcheting behavior of pressurized piping elbows subjected to in-plane moments

S. J. Zakavi*, B. Shiralivand, and M. Nourbakhsh

Faculty of Mech.Eng, Mohaghegh Ardabili, Ardabil, Iran

Article info:

Received: 18/10/2015
Accepted: 07/05/2016
Online: 15/07/2017

Keywords:
Ratcheting,
Pressurized elbow pipe,
In-plane bending moment,
Strain hardening,
Finite element.

Abstract

In this paper, the ratcheting behavior of carbon steel (ASTM A106B) and stainless steel (304L) elbows is studied under steady internal pressure and in-plane external moments at frequencies typical of seismic excitations. The finite element analysis with the nonlinear isotropic/kinematic (combined) hardening model is used to evaluate ratcheting behavior of the elbows. Material parameters are obtained from several stabilized cycles of specimens that are subjected to symmetric strain cycles. The rate of ratcheting depends significantly on the magnitudes of the internal pressure, dynamic bending moment and material constants for combined hardening model. The results show that the maximum ratcheting occurs in the hoop direction at the crown. Also, the results show that initially, the calculated rate of ratcheting is large and then decreases with the increasing cycles. Also, the results obtained by using the combined hardening model gives acceptable adaptation in comparison with the other hardening models (AF and Chaboche hardening models); however, this model gives overestimated values comparing with the experimental data.

Notation

t	Thickness
D_0	Outside diameter
E	Young's modulus
M	Dynamic bending moment
M_L	Limit moment of elbow
M_y	Yield moment
$M_{P0.2}$	0.2% collapse moment
P	Internal pressure
P_d	Design pressure
S_m	Allowable design stress intensity
y	Thickness correction factor = 0.4
σ_{ult}	Tensile stress
σ_y	Yield stress
σ^0	Instantaneous yield surface size
σ	Stress tensor
X	Back stress tensor
k	Initial size of the yield surface
R	Isotropic hardening parameter
b, Q	Material constants for isotropic hardening
C, γ	Material constants for kinematic hardening
ε^P	Plastic strain tensor
ε_P	Equivalent plastic strain

Corresponding author
email address: zakavi@uma.ac.ir

1. Introduction

Pressurized piping elbows are important parts in chemical industries and power plant components. The plastic strain accumulation occurs in these pressurized components under cyclic loading with non-zero mean stress. This progressive plastic deformation is called ratcheting strain. Ratcheting can cause failure in components through cracking or plastic buckling. Thus, in designing of pressurized piping elbows in power plant industries, accurate simulation of the plastic strain rate in each cycle is important. The literature review shows that accurate closed-form solutions may not be found to analyze the ratcheting behavior of the pressurized pipes under cyclic bending loading which can be caused by seismic loads. However, a great number of cyclic plasticity constitutive models have been proposed and developed for ratcheting response simulations of materials such as Chaboche and his co-workers models [1-4], Ohno and Wang models [5-6], as well as Ohno [7], Hassan and Kyriakides [8], Hassan et al. [9], Hassan and Kyriakides [10,11], AbdelKarim and Ohno [12], Bari and Hassan [13-15], Chen et al. [16-21] plasticity models. Many efforts have been made to understand the ratcheting phenomena. Some experimental works to study the ratcheting of the piping system have been carried out by EPRI (English [22], Ranganath, Hwang and Tagart [23]), Yahiaoui et al. [24-29], Hassan et al. [8-11,30], Igaria et al. [31], Feaugas and Gaudin [32], Chen et al. [16,17].

Recent experimental and numerical progress of the structural ratcheting for various piping components have been reviewed in reference [21]. Chen et al. [16,17,21] experimentally studied multiaxial ratcheting for pressurized low carbon steel elbow under reversed bending. It was shown that the maximum ratcheting strain occurs mainly in the hoop direction at flanks. Tasnim, et al. [8,9] discussed the ratcheting behavior of CS1020 and CS1026 carbon steels under stress-controlled cyclic loading. The influences of mean stress and stress amplitude on ratcheting were evaluated. Bari and Hassan [13-15] studied several kinematic hardening models to identify or develop a kinematic hardening rule that works well for ratcheting prediction on steels. Yahiaoui et al. [28] tested eight pairs of carbon and stainless steel, long and short radius welding elbows under conditions of steady internal pressure and in-plane, resonant dynamic moments to simulate seismic excitations. It was shown that the maximum ratcheting strain occurs at crown and intrados positions for in-plane bending.

2. Materials and methods

In this paper, a finite element code, ABAQUS, is used to study the ratcheting of carbon steel (ASTM A106B) and stainless steel (304L) pressurized elbows subjected to in-plane bending moments. In the experimental tests [28], series of tests are undertaken subjecting pressurized elbow specimens to rise amplitude dynamic (5 Hz, the resonant frequency) bending moments. Then, by conducting a series of finite element runs based on the nonlinear isotropic/kinematic hardening model using the ABAQUS, the experimental tests are modeled and ratcheting data obtained. Then the two sets of results are compared with each other and with the AF [33] and Chaboche hardening models [34].

3. Hardening model

The hardening models are used to simulate the inelastic behavior of materials that are subjected to cyclic loading. The kinematic hardening model describes the translation of the yield surface in the stress space and the isotropic hardening model describes the change of the elastic range. The isotropic hardening behavior of the model defines the evolution of the yield surface size R as a function of the equivalent plastic strain ε_P [34]:

$$\mathrm{d}R = b(Q - R)\mathrm{d}\varepsilon_P \tag{1}$$

where Q and b are two material coefficients. Integrating the above equation with the initial value $R = 0$ and considering yield surface equation gives:

$$\sigma^0 = k + Q[1 - \exp(-b.\varepsilon_p)] \quad (2)$$

where σ^0 is the instantaneous yield surface size and k is the yield stress at zero plastic strain. Here, Q is the maximum change in the size of the yield surface and b defines the rate at which the size of the yield surface changes as plastic strain develops.

The nonlinear kinematic hardening model was first proposed by Armstrong- Frederick [34].

$$dX = \frac{2}{3} C\, d\varepsilon^P - \gamma X\ d\varepsilon_P \quad (3)$$

where X is the back stress tensor, $d\varepsilon_P$ is the equivalent plastic strain rate, C and γ are two material dependent coefficients in the Armstrong-Frederick kinematic hardening model. The evolution equation of hardening can be integrated analytically to give:

$$X = \nu \frac{C}{\gamma} + (X_0 - \nu \frac{C}{\gamma}) \exp[-\nu\gamma(\varepsilon_P - \varepsilon_{P0})] \quad (4)$$

where $\nu = \pm 1$ according to the direction of flow, and ε_{P0} and X_0 are the initial values, For example at the beginning of each plastic flow.

The evolution law of combined model consists of two components: a nonlinear kinematic hardening component, which describes the translation of the yield surface in the stress space through the back stress X, and an isotropic hardening component, which describes the change of the equivalent stress defining the size of the yield surface R as a function of plastic deformation. When temperature and field variable dependencies are omitted, the hardening law is:

$$dX = C \frac{1}{R}(\sigma - X) d\varepsilon_P - \gamma X\ d\varepsilon_P \quad (5)$$

4. Material experiments and model parameters determination

The experimental test for determination of hardening parameters has been reported in reference [35].It is sufficient to give a brief outline of the technique. The calibration procedure consists of several cylindrical bar tests, one of which is subjected to monotonic tension until necking and others are under symmetric strain-controlled experiments with different strains. From symmetric strain-controlled experiments, the plastic strain equals to the summation of the absolute value of the change in longitudinal plastic strains:

$$\bar{\varepsilon}_p = \sum_i \left|\Delta\varepsilon_{p(i)}\right| = \sum_i \left|\Delta\varepsilon_i - \Delta\bar{\sigma}_{\exp} / E\right| \quad (6)$$

where ε_i total strain, $\bar{\sigma}_{\exp}$ is the measured stress and E is the elastic modulus.

A typical curve for stabilized cycles in a strain-controlled test on SS304L is shown in Fig. 1.

The equivalent back stress, $\bar{X}$, equals to one-half of the difference in yield stress between the end of the tensile loading and first yield of the subsequent compressive loading.

These results, corresponding $(\bar{X}, \bar{\varepsilon}_p)$ data pairs, may be plotted, and the kinematic hardening parameters, C and γ, may be calculated by fitting Equation (4) to the data and selecting parameters to minimize the sum of the square of the error between Equation (4) and the data. A typical curve-fit data for C and γ calibration is shown in Fig. 2.

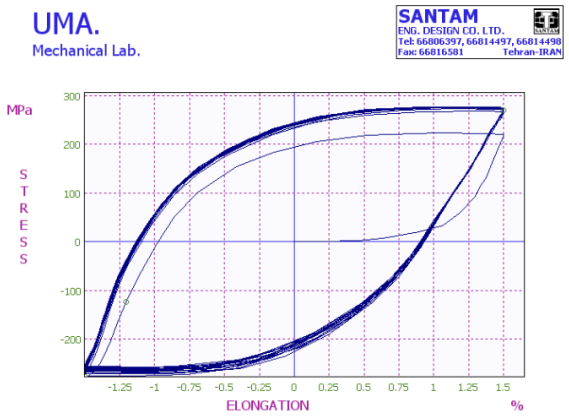

Fig. 1. The stabilized cycles in a strain-controlled test on SS304L.

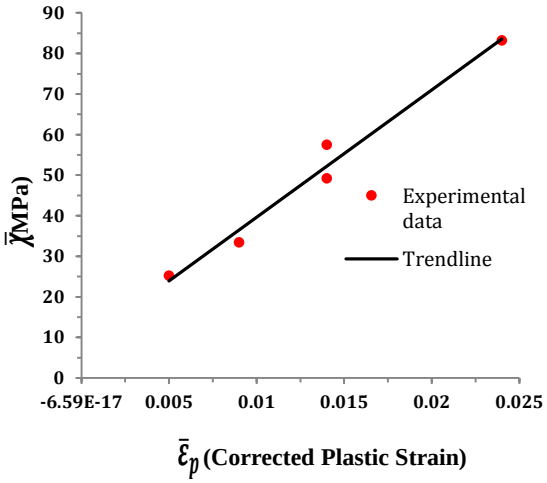

Fig. 2. Curve-fit data for C and γ calibration (SS304L).

The results from monotonic tension test are used to determine the experimental equivalent stress versus equivalent plastic strain data up until the point of necking. Using the experimental data from one-half of the necking strain until the necking strain, the monotonic hardening curve, (Equation (7)), is fit to the data using nonlinear least-squares regression.

$$\bar{\sigma} = \sigma_y (1 + \frac{\bar{\varepsilon}_p}{m})^n \tag{7}$$

In this equation, $\bar{\sigma}$ is the equivalent stress, σ_y is the initial uniaxial yield stress, and m and n are material constants. Upon fitting Equations (4) and (7) to the experimental data, $\bar{\sigma}$ and $\bar{X}$ are known for any equivalent plastic strain, and the isotropic component of the hardening, σ^0, may be defined as a function of equivalent plastic strain by:

$$\sigma^0(\bar{\varepsilon}_p) = \bar{\sigma}(\bar{\varepsilon}_p) - \bar{X}(\bar{\varepsilon}_p) \tag{8}$$

The isotropic material parameters, Q and b, can be determined by fitting Equation (2) to the results of Equation (8) and using least squares nonlinear regression. A typical curve-fit data for Q and b calibration is shown in Fig. 3.

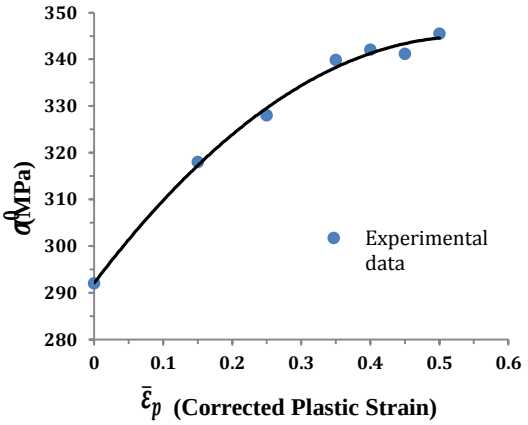

Fig. 3. Curve-fit data for Q and b calibration (SS304L).

For the carbon and stainless steels, the specification and properties obtained by tensile tests are given in Table 1. The kinematic and isotropic hardening parameters for the carbon and stainless steels are [$C = 2763.69$ MPa , $\gamma = 17.66$, $Q = 135.9$MPa and $b = 4.76$] and [$C = 3941.31$MPa , $\gamma = 15.85$, $Q = 98.11$MPa and $b = 1.47$], respectively.

5. Review of experimental and FE arrangement

The experimental set-up for testing piping elbows under in-plane bending has been reported in reference [28] and it is sufficient to give a brief outline of the technique. The nominal pipe size is 2 inches NPS corresponding to an outside diameter of 60.3 mm. The component identification and relevant dimensions of the elbows are given in Table 2. The parameters and section of the experimental results is shown in Fig. 4. Pairs of 90° welding elbows [28] are, for symmetry, tested simultaneously as shown in Fig. 5. To obtain natural frequencies typical of seismic excitations (i.e. below 10 Hz), lumped masses are attached to straight tangents (lateral limbs), thus making the test assembly resemble a double cantilever configuration. All tests reported here are performed in a servo hydraulic testing machine fitted with a fatigue module. In this testing program, the maximum displacement of the input ram is limited to 10 mm. The test components are pressurized independently by

hand-pumped oil to their design pressure, calculated using the ASME Code formula. The internal pressure is kept constant during testing. Next, in the FE arrangement, the dynamic load to induce the cyclic bending is applied at the end nodes of the simulation model. It is specified as a sinusoidal force with a circular frequency. The frequency and design pressure of elbows is given in Table 3. At the positions of peak stress to assess the ratcheting behavior of the components, the stresses on the outside and inside surfaces are of equal magnitude but of opposite sign and that the peak stresses occur at the crown of the elbows in the hoop direction for the long radius elbows. On testing the first short radius geometry, failure is occurred by a crack running in the hoop direction at the intrados. Therefore, the gauge displaces from the flank to the intrados of the elbows for the short radius [28].

For all specimens, the finite element code, ABAQUS, is used to study ratcheting behavior of pressurized elbows under simulated seismic bending moments. The elbow specimen model under pressure and the cyclic bending moment is shown in Fig. 6. The elbows have a 1.50 m long pipework modeled by 4800 elements. The type of elements used in the FE analysis is C3D8R. The number of elements used in the middle part of model and lateral are 4800 and 1640 elements, respectively. The latter numbers of elements and element type are decided after a series of solution convergence runs. The displacements in all three directions and twisting about the pipe axis are prevented at the nodes.

Table 1. Material properties obtained by tensile tests.

	Carbon steel (ASTM A106B)	Stainless steel (304L)
Young's modulus	214GPa	200GPa
Ultimate stress	475MPa	597MPa
2% proof stress	328MPa	292MPa
Elongation at failure (%)	42%	81%
$S_m = \min(\sigma_{ult}/3, 2\sigma_Y/3)$	158MPa	193MPa

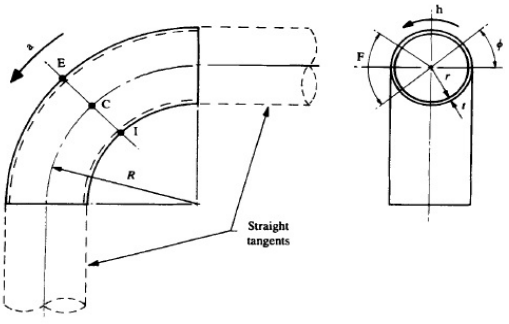

Fig. 4. Elbow geometry, stress directions, angular coordinate and definition of important locations around the bend [28].

a = Axial direction
h = Hoop direction
ϕ = Angular position around mid-circumference section containing E, C and I= 0° at C and positive towards E
C = Crown positions (ϕ = 0°, 180°)
E = Extrados (ϕ = +90°)
F = Flank regions (defined by ϕ = ±45° about the crowns)
I = Intrados (ϕ = -90°)

Table 2. Component identification and geometry (Carbon steel-Stainless steel) [28].

Component identification*	Thickness (mm), (schedule)	Bend Radius (mm)	Bend characteristic H = t R/r2	Radius ratio b = R/r
CLSI (SLSI)	3.91, (40)	76	0.37	2.7
CLXI (SLXI)	5.54, (80)	76	0.56	2.8
CSSI (SSSI)	3.91, (40)	51	0.25	1.8
CSXI (SSXI)	5.54, (80)	51	0.38	1.9

*Components are labelled by a four-character coding; First character: C for carbon or S for stainless steel; Second character: L for long or S for short radius bends; Third character: S for standard weight or X for extra strong; Fourth character: I is used here to denote in-plane bending

Table 3. The frequency and design pressure.

Component identification*	Frequency (Hz)	Design pressure (MPa)
CLSI(SLSI)	3.81(3.99)	18.9(15.8)
CLXI(SLXI)	4.02(4.11)	27.4(22.8)
CSSI(SSSI)	4.13(3.92)	18.9(15.8)
CSXI(SSXI)	4.20(4.25)	27.4(22.8)

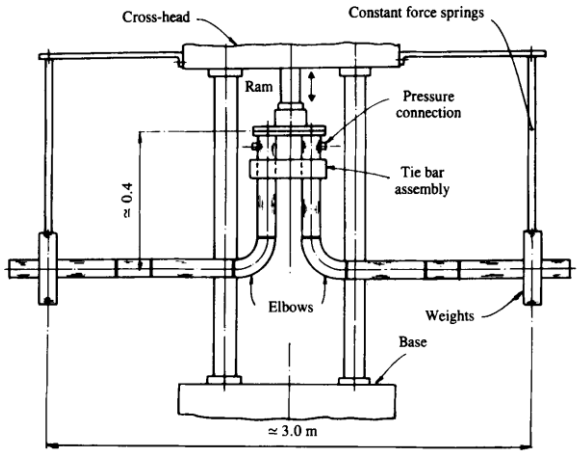

Fig. 5. Elbow testing fixture in-plane bending [28].

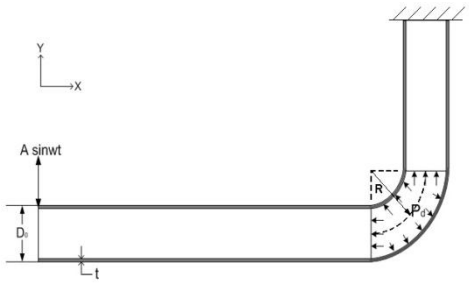

Fig. 6. Elbow specimen model under pressure and cyclic bending moment.

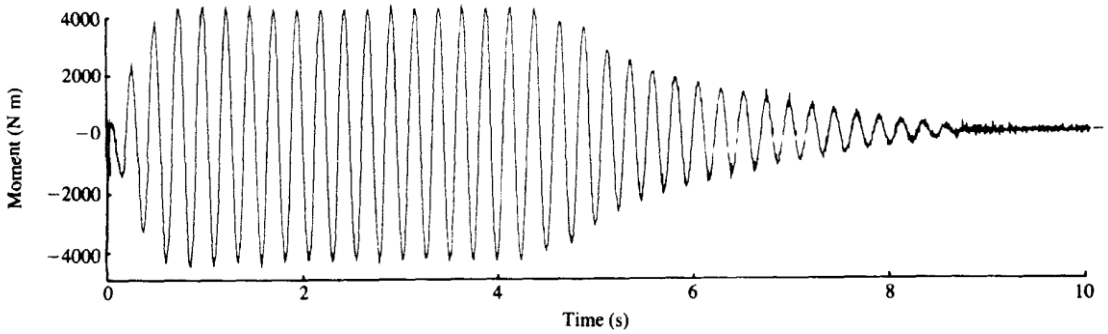

Fig. 7(a). Experimental response moment/time (CLXI).

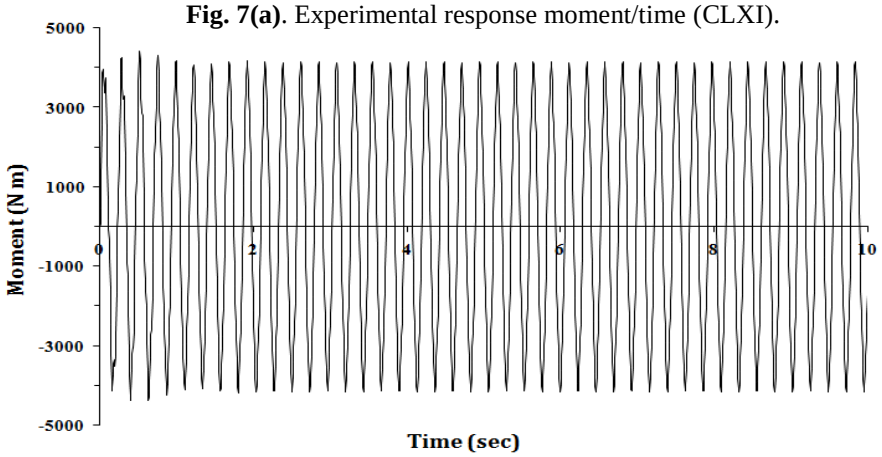

Fig. 7(b). FE response moment/time (CLXI).

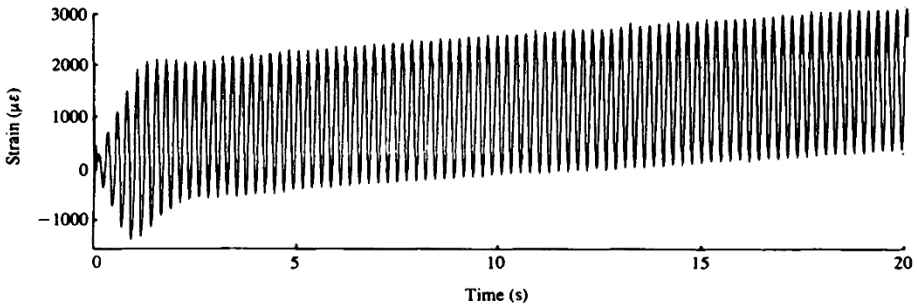

Fig. 8(a). Experimental strain response in presence of ratcheting of component CSSI at a dynamic bending moment of 5987.45Nm.

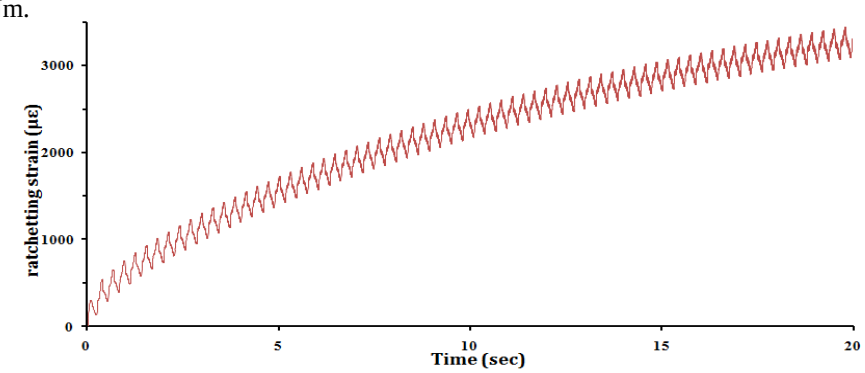

Fig. 8(b). FE strain response in presence of ratcheting of component CSSI at a dynamic bending moment of 5987.45Nm.

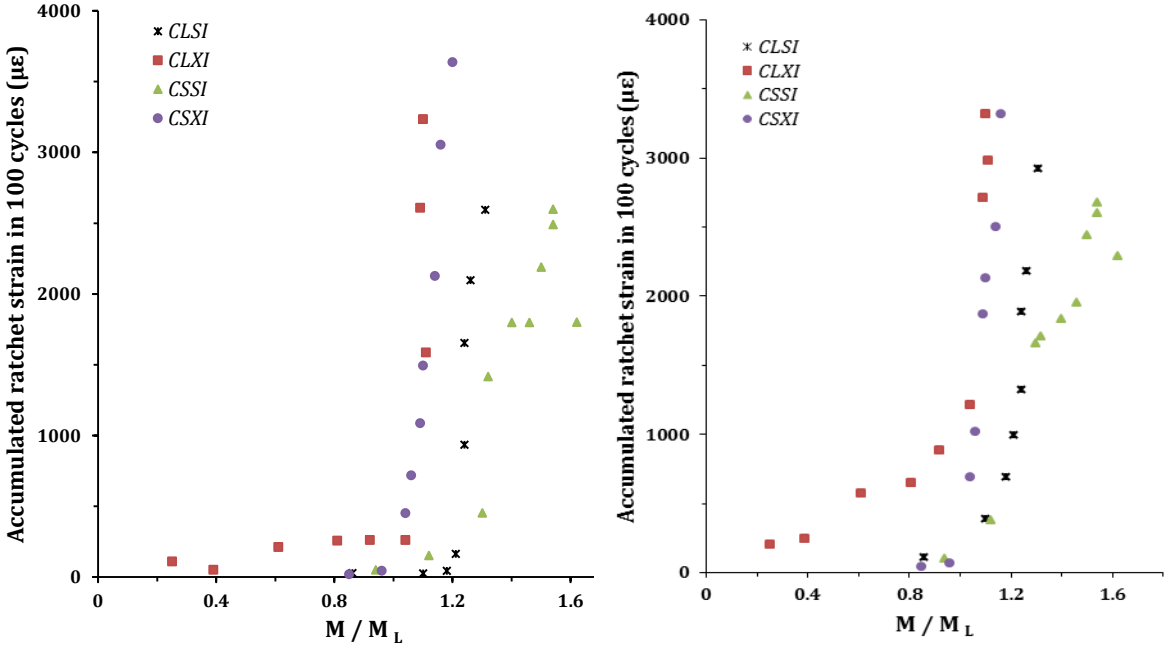

Fig. 9. (a) Experimental ratcheting data [28] and (b) FE analysis against ratios of applied to limit moments for components CS.

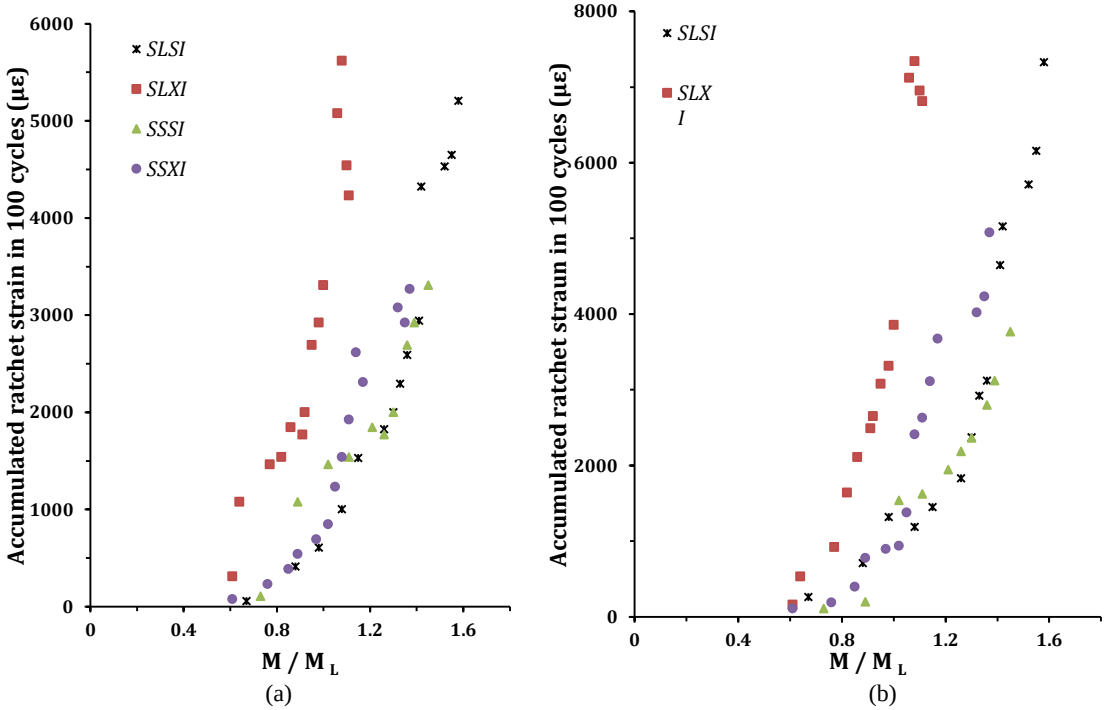

Fig. 10. (a) Experimental ratcheting data [28] and (b) FE analysis against ratios of applied to limit moments for components SS.

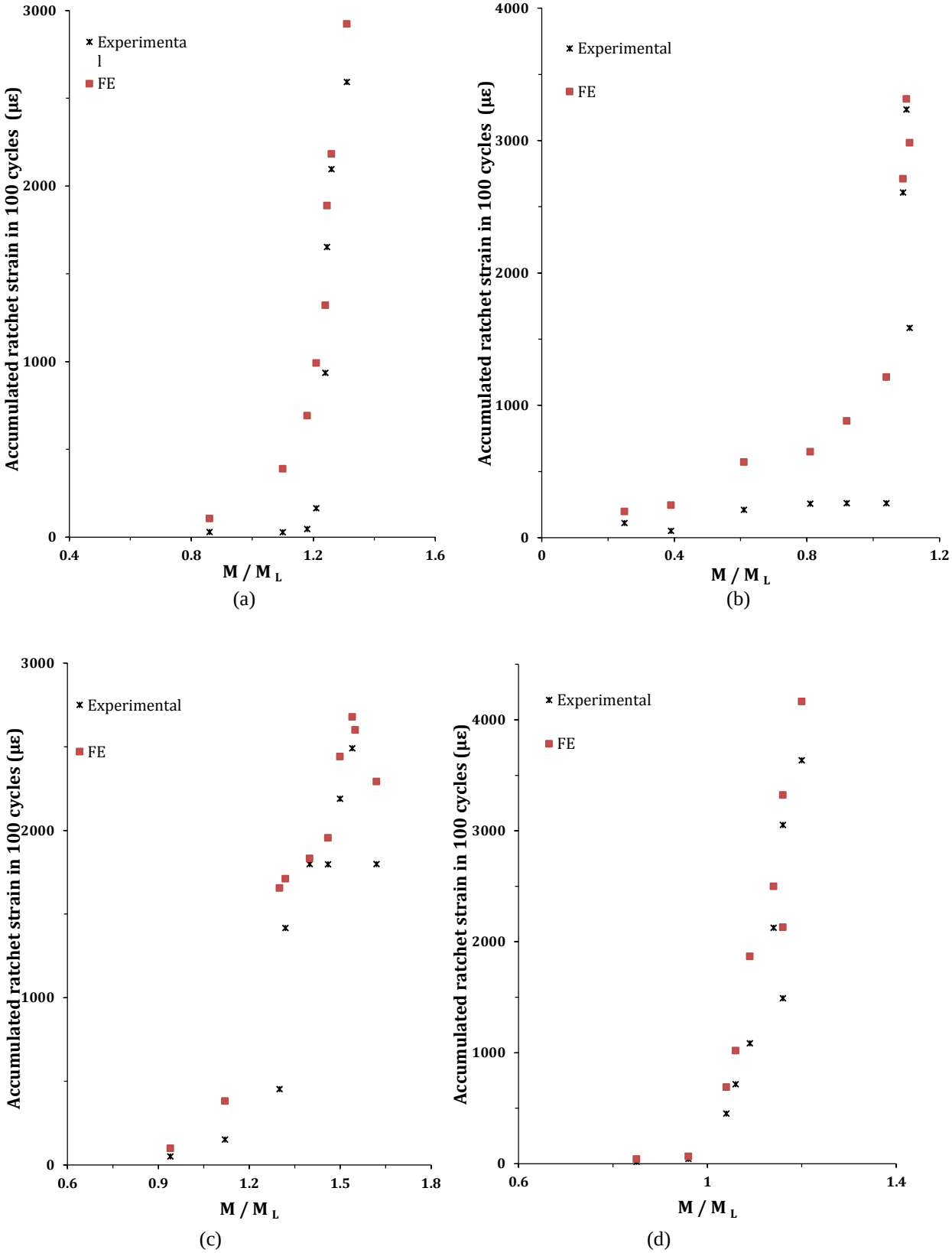

Fig. 11. Experimental and FE ratchet strains for the specimens; (a) CLSI, (b) CLXI, (c) CSSI, and (d) CSXI.

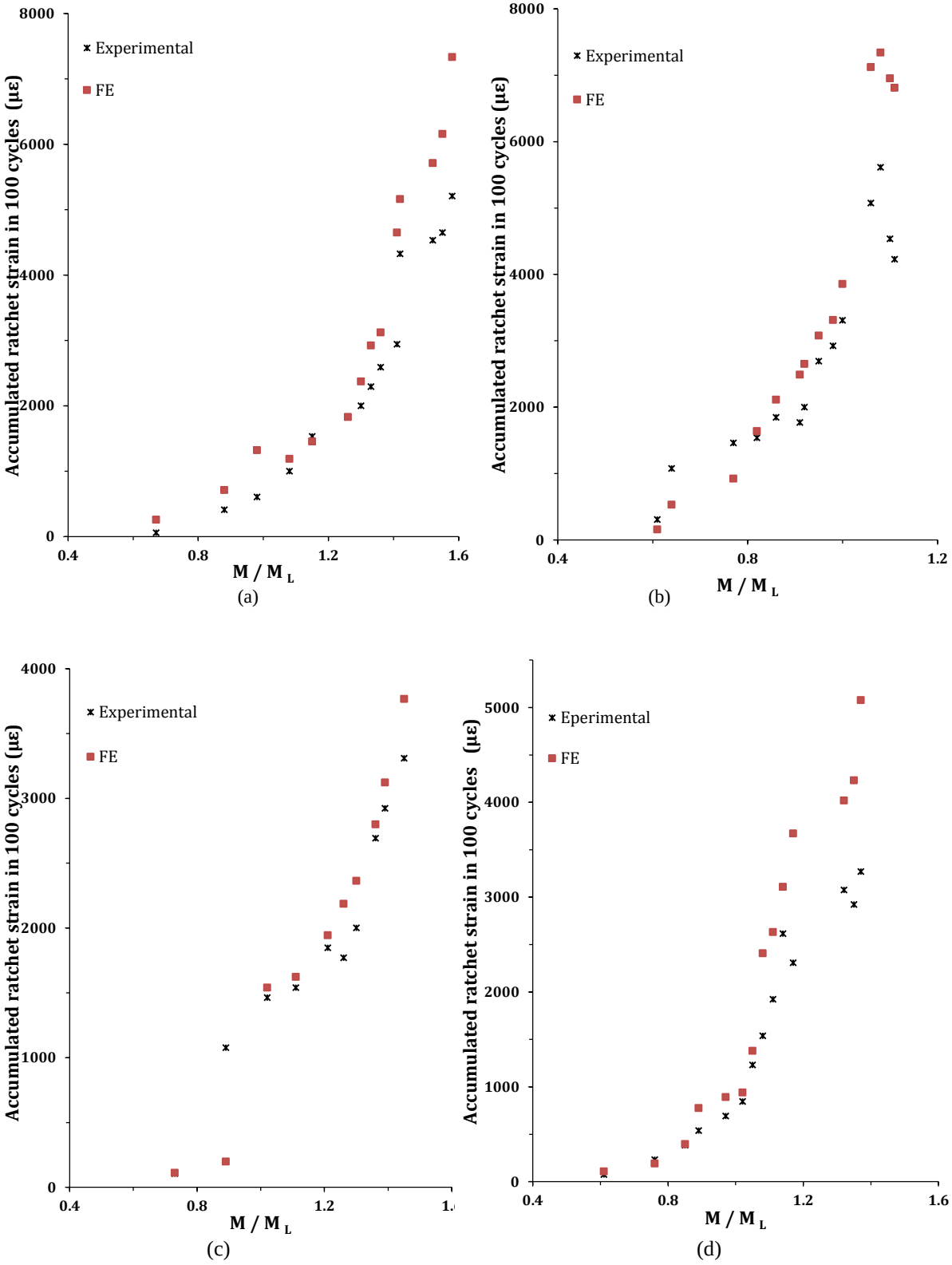

Fig. 12. Experimental and FE ratchet strains for the specimens; (a) SLSI, (b) SLXI, (c) SSSI, and (d) SSXI.

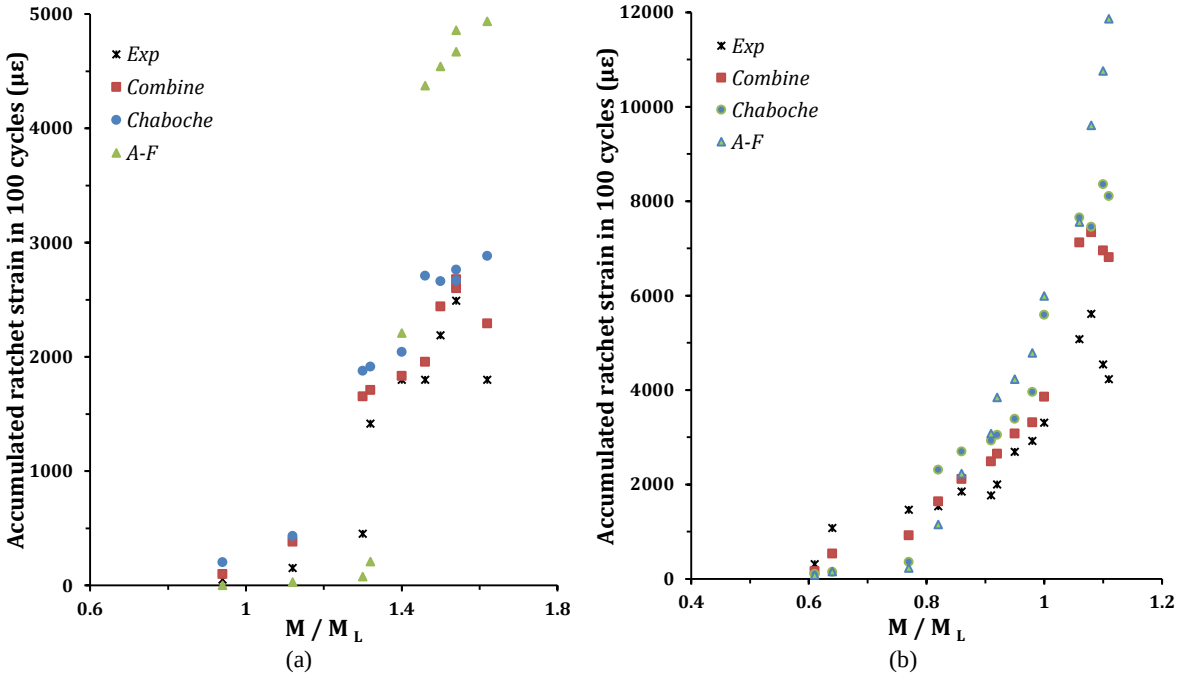

Fig. 13. (a) Experimental and FE ratchet strains for the specimen CSSI and (b) SLXI.

7. Experimental and FE results

Detailed results are presented for two of the specimens tested (CSSI and SLXI) and summary results are given for all tests conducted.

In Fig. 7(a, b) traces of the response moment are presented for a typical test on component CLXI. These clearly show that a reasonably stable bending moment response is achieved for the duration of the test in this case up to 10s. A typical hoop strain response is extracted from the experimental and FE analysis for the CSSI component is presented in Fig. 8.

The results obtained from all experimental ratcheting tests and from FE analysis for all components are plotted in Figs. 9(a, b) and 10(a, b). Here, the strain for each cycle is calculated as the average over the period of the test and plotted against $M / M_{0.2}$. Figures 8 and 9 show the data recorded for the outside surface.

A typical set of results for carbon steel specimens is shown in Fig. 11, which includes results from the FE analysis using the combined hardening model. Here, the ratchet strain per cycle averaged over the first 10s of excitation is plotted against increasing M / M_L ratios for the experimentally obtained data and the finite element data (M_L is the moment based on proof stress $\sigma_{0.2} = 242MPa$). For both experimental data and the finite element results, the ratchet strains are shown. The same information obtained for the stainless steel specimens are illustrated in Fig. 12.

The experimental and FE results illustrated by Fig. 9(a, 9) show the onset of ratcheting for the stainless steel elbow specimens occur at $0.6 \le M / M_L \le 0.7$ and $0.61 \le M / M_L \le 73$, respectively. Also, the experimental and FE results illustrated from Fig. 10(a, b) show the onset of ratcheting for the carbon steel elbow specimens occur at $1 \le M / M_L$ and $0.85 \le M / M_L \le 0.94$, respectively. It is evident from Figs. 9-12 that the hoop strain ratcheting rates predicted by the FE using combined hardening model are near those are found experimentally. Also, M / M_L ratios for the onset of ratcheting in the stainless steel specimens are less than those of the equivalent

carbon steel elbows. The results show that the ratcheting for the stainless steel elbows is greater than those of the equivalent carbon steel elbows. Fig.13 shows that the results obtained by using the combined hardening model gives an acceptable adaptation in comparison with the other hardening models (AF and Chaboche hardening models) when compared to the experimental data.

Table 4. Experimental and FE ratcheting data for the specimen CSSI.

Dynamic bending moment M (N.m)	M/M_L	Experimental ratcheting data ($\mu\varepsilon$/cycle)	FE (A-F) ratcheting data ($\mu\varepsilon$/cycle)	FE (Chaboche) ratcheting data ($\mu\varepsilon$/cycle)	FE (Combined) ratcheting data ($\mu\varepsilon$/cycle)
3060.35	0.94	51.67	203.10	0.30	98.97
3820.67	1.12	151.63	432.40	29	382.20
4439.11	1.30	453.20	1879	77.65	1655
4508.34	1.32	1416.08	1913	208.7	1711
4705.33	1.40	1798.90	2043	2209	1832
4908.67	1.46	1798.06	2709	4372.20	1955
5049.07	1.50	2189.31	2661	4541.55	2441
5255.06	1.54	2598.13	2669	4669.71	2601
5320.78	1.54	2490.77	2763	4858.8	2679
5588.36	1.62	1799.49	2882	4937.07	2292

Table 5. Experimental and FE ratcheting data for the specimen SLXI.

Dynamic bending moment M (N.m)	M/M_L	Experimental ratcheting data ($\mu\varepsilon$/cycle)	FE (A-F) ratcheting data ($\mu\varepsilon$/cycle)	FE (Chaboche) ratcheting data ($\mu\varepsilon$/cycle)	FE (Combined) ratcheting data ($\mu\varepsilon$/cycle)
4090.91	0.61	307.69	76.85	97.66	159.10
4704.55	0.64	1076.92	153.70	143.94	531.20
5113.64	0.77	1461.54	230.55	357.88	922.50
5454.55	0.82	1538.46	1152	2312	1639
5727.27	0.86	1846.15	2228.52	2699	2111
6000	0.91	1769.23	3074.63	2924	2489
6136.36	0.92	2000	3842.65	3047	2651
6272.73	0.95	2692.31	4226.42	3391	3079
6477.27	0.98	2923.10	4783	3956	3314
6681.82	1.00	3307.69	5994.54	5593	3855
7090.91	1.06	5076.92	7561	7654	7123
7159.10	1.08	5615.38	9607	7455	7341
7227.27	1.10	4538.46	10756	8361	6953
7363.64	1.11	4230.77	11862	8109	6811

In Table 4, the ratchet strains found experimentally over a 10s test period and by FE analysis, for the same period, for the specimen CSSI are summarized. Table 5 gives the equivalent information for the specimen SLXI.

8. Conclusions

The experimental work reported here provides reliable data which can be used to judge the FE analysis using the ABAQUS package. However, it should be noted that the experimental work uses a rising amplitude technique which may effectively reduces the ratchet strain at any particular dynamic bending moment. It is possible that those tests conducted at low amplitude harden the material sufficiently to reduce the ratchet strains observed at higher amplitudes. It is not possible to quantify the possible magnitude of this effect. This possible effect would not influence the dynamic bending moment at which ratcheting is first observed. Typical data obtained experimentally and from FE model for all specimens are shown in Figs. 10-12. The experimental and FE results illustrated by Fig. 9(a, b) show the onset of

ratcheting for the stainless steel elbow specimens occur at $0.6 \le M / M_L \le 0.7$ and $0.61 \le M / M_L \le 73$, respectively. Also, the experimental and FE results illustrated by Figs 10a and 10b show the onset of ratcheting for carbon steel elbow specimens occur at $1 \le M / M_L$ and $0.85 \le M / M_L \le 0.94$, respectively. Complete sets of data for all specimens are plotted in Figs.10-11. Also, M / M_L ratios for the onset of ratcheting in the stainless steel specimens are less than those of the equivalent carbon steel elbows. The results show that the ratcheting for the stainless steel elbows is greater than those of the equivalent carbon steel elbows.

The important conclusion of this paper is to show the properties of nonlinear isotropic/kinematic hardening model to predict the cyclic loading behavior of the structures. In this study, stress-strain data and the material parameters are obtained from several stabilized cycles of the specimens that are subjected to symmetric strain cycles. Both experimental results and the FE analysis agree that ratcheting is influenced by the material stress-strain curve and load history. The rate of ratcheting depends significantly on the magnitudes of the internal pressure, dynamic bending moment and the material constants for combined hardening model. The results show that initially, the calculated rate of ratcheting is large and then decreases with the increasing the cycles. The FE model predicts that the hoop strain ratcheting rate is near to that found experimentally in all cases in which $M / M_L \le 1$. In addition, the results show that the FE method gives overestimated values comparing with the experimental data. According to the present model, the results obtained from FE method is near to those found from the experimental data comparing with the other hardening models (AF and Chaboche).

Acknowledgments

Appreciation is expressed to the technical staff of the Applied Mechanics Division of the Department of Mechanical Engineering at the University of Mohaghegh Ardabili (Iran) for their assistance with the work.

References

[1] J. L. Chaboche, "Time-independent constitutive theories for cyclic plasticity", *Int. J. of Plasticity*, Vol. 2, No. 2, pp.149-188, (1986).

[2] J. L. Chaboche, "On some modifications of kinematic hardening to improve the description of ratcheting effects". *International Journal of Plasticity*, Vol. 7, No. 7, pp. 661–678, (1991).

[3] J. L. Chaboche, "Modeling of ratcheting: evaluation of various approaches". *European Journal of Mechanics, A/Solids*, Vol. 13, No. 13, pp. 501–518, (1994).

[4] J. L. Chaboche , "A review of some plasticity and viscoplasticity constitutive theories", *Int. J. of Plasticity*, Vol. 24, No. 10, pp. 1642–1963, (2008).

[5] N. Ohno, and J. D. Wang, "Kinematic hardening rules with critical state of dynamic recovery, part I: formulations and basic features for ratcheting behavior". *International Journal of Plasticity*, Vol. 9, No. 3, pp. 375–390, (1993a).

[6] N. Ohno, and J. D. Wang , "Kinematic hardening rules with critical state of dynamic recovery, Part II: application to experiments of ratcheting behavior". *International Journal of Plasticity*, Vol. 9, No. 3, pp. 391–403, (1993b).

[7] N. Ohno, "Constitutive modeling of cyclic plasticity with emphasis on ratcheting". *International Journal of Mechanics and Sciences*, Vol. 40, No. 2-3, pp. 251–261, (1998).

[8] T. Hassan, and S. Kyriakides, "Ratcheting in cyclic plasticity, part I: uniaxial behavior", *International Journal of Plasticity*, Vol. 8, No. 1, pp. 91–116, (1992).

[9] T. Hassan, E. Corona, and S. Kyriakides, "Ratcheting in cyclic plasticity, Part II: multiaxial behavior", *International Journal of Plasticity*, Vol. 8, No. 2, pp. 117-146, (1992).

[10] T. Hassan, and S. Kyriakides, "Ratcheting of cyclically hardening and softening materials, Part I: uniaxial behavior", *International Journal of Plasticity*, Vol. 10, No. 2, pp. 149–184, (1994a).

[11] T. Hassan, and S. Kyriakides, "Ratcheting of cyclically hardening and softening materials, Part II: multiaxial behavior". *International Journal of Plasticity*, Vol. 10, No. 2, pp. 185-212, (1994b).

[12] M. Abdel Karim, and N. Ohno, "Kinematic hardening model suitable for ratcheting with steady-state", *International Journal of Plasticity*, Vol. 16, No. 3, pp. 225-240, (2000).

[13] S. Bari, and T. Hassan, "Anatomy of coupled constitutive model for ratcheting simulation", *International Journal of Plasticity*, Vol. 16, No. 3-4, pp. 381-409, (2000).

[14] S. Bari, and T. Hassan, "Kinematic hardening rules in uncoupled modeling for multiaxial ratcheting simulation", *International Journal of Plasticity*, Vol. 17, No. 7, pp. 885-905, (2001).

[15] S. Bari, and T. Hassan, "An advancement in cyclic plasticity modeling for multiaxial ratcheting simulation", *International Journal of Plasticity*, Vol. 18, No. 7, pp. 873–894, (2002).

[16] X. Chen, B. Gao, and G. Chen, "Multiaxial ratcheting of pressurized elbows subjected to reversed in-plane bending", *J. Pres. Eq. Syst.*, Vol. 3, No. 3, pp. 38-44, (2005).

[17] X. Chen, B. Gao, and G. Chen, "Ratcheting study of pressurized elbows subjected to reversed in-plane bending", *J. of Pressure Vessel Technology*, Vol. 128, No. 4, pp. 525-532, (2006).

[18] X. Chen, R. Jiao, and K. S. Kim, "Simulation of ratcheting strain to a high number of cycles under multiaxial loading", *International Journal of Solids and Structures*, Vol. 40, No. 26, pp. 7449-7461, (2003).

[19] X. Chen, and R. Jiao, "Modified kinematic hardening rule for multiaxial ratcheting prediction", *International Journal of Plasticity*, Vol. 20, No. 4-5, pp. 871-898, (2004).

[20] X. Chen, R. Jiao, and S.K. Kwang, "On the Ohno–Wang kinematic hardening rules for multiaxial ratcheting modeling of medium carbon steel", *Int. J. of Plasticity*, Vol. 21, No. 1, pp. 161-184, (2005).

[21] X. Chen, Xu. Chen, D. Yu, and B. Gao, "Recent progresses in experimental investigation and finite element analysis of ratcheting in pressurized piping", *Int. J. of Pressure Vessels and Piping* , Vol. 101, No. 1, pp. 113–142, (2013).

[22] W. F. English, "Piping and fitting dynamic reliability program-fourth semi-annual progress report" Nov. 1986-Apr.1987,GE Nuclear Energy, NEDC-31542, (1988).

[23] S. Ranganath, H. Hwang, and S. W. Tagart, "Piping and fitting dynamic reliability program". EPRI Nuclear Power Division, (1989).

[24] K. Yahiaoui, D. G. Moffat, and D. N. Moreton, "Techniques for the investigation of the ratcheting behavior of piping components under internal pressure and simulated seismic loading", *BSSM J. strain*, Vol. 28, No. 2, pp. 53-90, (1992).

[25] K. Yahiaoui, D. G. Moffat, and D. N. Moreton, "Single frequency seismic loading tests on pressurized branch pipe intersections machined from solid", *J. of strain Analysis*, Vol. 28, No. 3, pp. 197-207, (1993).

[26] K. Yahiaoui, D. G. Moffat, and D. N. Moreton, "Stress Limits for Pressurized Piping Branch Junctions Under In-Plane Run pipe Simulated Seismic Loadings". *ASME J. Pressure Vessel Tec*, Vol. 116, No. 2, pp. 150–160, (1994).

[27] K. Yahiaoui, D. G. Moffat, and D. N. Moreton, "Cumulative damage assessment at pressurized piping branch junctions under in- plane run pipe simulated seismic bending", *Int. J. pres. ves. piping*, Vol. 63, No. 2, pp. 119–128, (1995).

[28] K. Yahiaoui, D. G. Moffat, and D. N. Moreton, "Response and cyclic strain accumulation of pressurized piping

elbows under dynamic in plane bending", *J. of strain analysis*, Vol. 31, No. 2, pp. 135–151, (1996).

[29] K. Yahiaoui, D. N. Moreton, and D. G. Moffat, "Response and cyclic strain accumulation of pressurized piping elbows under dynamic out-of- plane bending", *J. of strain analysis*, Vol. 311, No. 2, pp. 153–166, (1996).

[30] T. Hassan, T. Lakhdar, and K. Shree, "Influence of non-proportional loading on ratcheting responses and simulations by two recent cyclic plasticity models", *Int. J. of Plasticity*, Vol. 24, No. 10, pp. 1863-1889, (2008).

[31] T. Igaria, M. Kobayashi, F. Yoshida, and S. Imatani, Inoue, T., "Inelastic analysis of new thermal ratcheting due to a moving temperature front", *International Journal of Plasticity*, Vol. 18, No. 9, pp. 1191-1217, (2002).

[32] X. Feaugas, and C. Gaudin, "Ratcheting process in the stainless steel AISI 316L at 300 K: An experimental investigation". *International Journal of Plasticity*, Vol. 20, No. 4, pp. 643-662, (2004).

[33] P. J. Armstrong, and C. O. Frederick, "A mathematical representation of the multi axial Bauschinger effect". CEGB Report RD/B/N 731, Central Electricity Generating Board. The report is reproduced as a paper: 2007, *Materials at High Temperatures*, Vol. 24, No. 1, pp. 1-26, (1966).

[34] J. L. Chaboche, "Constitutive equations for cyclic plasticity and cyclic viscoplasticity". *Int. J. of Plasticity*, Vol. 5, No. 3, pp. 247-302, (1989).

[35] S. J. Zakavi, M. Zehsaz, and M. R. Eslami, "The ratcheting behavior of pressurized plain pipework subjected to cyclic bending moment with the combined hardening model", *Nuclear Engineering and Design*, Vol. 240, No. 4, pp. 726-737, (2010).

How to cite this paper:

S. J. Zakavi, B. Shiralivand, and M. Nourbakhsh," Evaluation of combined hardening model in ratcheting behavior of pressurized piping elbows subjected to in-plane moments", Journal of Computational and Applied Research in Mechanical Engineering, Vol. 7. No. 1, pp. 57-71

DOI: 10.22061/JCARME.2017.640
URL: http://jcarme.srttu.edu/article_640.html